KERNFORSCHUNGSZENTRUM

KARLSRUHE

August 1966

KFK 474

Institut für Neutronenphysik und Reaktortechnik

Special Experimental Techniques Developed Recently for Application in Fast Zero Power Assemblies

A. Bayer, H. Seufert, D. Stegemann

GESELLSCHAFT FÜR KERNFORSCHUNG M. B. H.

KARLSRUHE

KERNFORSCHUNGSZENTRUM KARLSRUHE

August 1966 KFK 474

Institut für Neutronenphysik und Reaktortechnik

SPECIAL EXPERIMENTAL TECHNIQUES DEVELOPED RECENTLY FOR APPLICATION IN FAST ZERO POWER ASSEMBLIES *

A.Bayer, H.Seufert, D.Stegemann

Paper presented at the International Conference on Fast Critical Experiments and their Analysis held at Argonne (Illinois), Oct. 10-13, 1966

* Work performed within the association in the field of fast reactors between the European Atomic Energy Community and Gesellschaft für Kernforschung m.b.H., Karlsruhe

Gesellschaft für Kernforschung m.b.H., Karlsruhe

ABSTRACT

A description and discussion of three different experimental methods are given, which were developed particularly for application in fast zero power assemblies.

The first method described deals with the absolute determination of ^{238}U capture rates. The principle is based upon the fact that ^{243}Am and ^{239}U decay via ^{239}Np into ^{239}Pu. The α-disintegration rate of ^{243}Am is determined absolutely by low geometry α-particle counting. From this the absolute ^{239}Np disintegration rate follows directly, which is measured by the 106 keV γ-x ray coincidence technique, so avoiding radiochemical separation. The γ-x ray self-attenuation within thick uranium foils is treated quantitatively and an optimum foil thickness is derived. Special attention has been given to the reduction and correction of background due to fission product γ-activity. A detailed error analysis shows an overall accuracy of about 1% for the absolute ^{239}Np disintegration rate including γ-attenuation effects within the foils.

The second method is concerned with the application of resonance activation foils in the keV-region, where, besides ^{23}Na, the application of ^{19}F and ^{27}Al was found to be interesting. Due to the short half lives of 11.5 sec (^{20}F) and 2.3 min (^{28}Al) an automatic rabbit-irradiation system was developed by which the irradiated foils were transported immediately between two detectors so that counting could be started 3 seconds after the end of irradiation. The calibration procedure for foils and detectors is given. An error analysis is also presented which showed that the accuracy is limited by the cross section data available at the present time.

The third method presented is used to determine the prompt neutron decay constant, the reactivity, and the absolute reactor power by investigation of the neutron noise. The probability distribution of detector counts in given time intervals is measured by a "proabability distribution analyzer". The specific feature of this technique is that the complete probability distribution of interest can be measured at once. The experimental set-up of the analyzer is described in detail. The derivation of reactor parameters from the measured distributions is discussed and the applicability of this technique to plutonium-fuelled fast reactor assemblies is mentioned.

1. METHOD FOR ABSOLUTE DETERMINATION OF ^{238}U-CAPTURE RATES

INTRODUCTION

The special feature of the method is the use of the ^{243}Am α-decay into ^{239}Np, which in turn decays to ^{239}Pu. The disintegration rate of ^{239}Np is measured by the well-known 106 keV γ-x ray coincidence technique (1, 2, 3). The ^{243}Am disintegration rate is absolutely measured by low geometry α-counting. The ^{243}Am-^{239}Np-^{239}Pu decay chain enables one, therefore, to obtain the absolute ^{239}Np disintegration rate.

Comparing this method to others applied so far to ^{238}U capture rate measurements in fast and thermal systems, we found certain characteristics. The first one is the obtainable accuracy of ca. 1% for the determination of absolute ^{239}Np disintegration rates, including the effect of γ-x ray self-attenuation within the uranium foils. For this accuracy achieved, the easy control of long time electronics stability by the constant ^{243}Am source is a necessity. The second characteristic is concerned with the suppression of γ-background due to fission fragment activity. This is of considerable importance in fast reactor assemblies because of the significant fraction of fast fission in ^{238}U. The application of the γ-x ray coincidence technique allows a successful reduction of fission-γ-background as has been shown by TUNNICLIFFE et al. (1). Experimental results obtained from foil irradiations in fast neutron spectra showed very clearly the superiority of the coincidence experiment over the single detector method in this respect. The third characteristic is that radiochemical separation of ^{239}Np with all its difficulties can be avoided.

A simultaneous determination of capture rates (^{238}U) and fission rates (^{239}Pu, ^{235}U, ^{238}U etc. according to type of foils) is also possible, if the fission product γ-rays of energy greater than 660 keV and the coincident 106 keV γ-x rays are counted in the same experimental run. The counting rate due to fission product γ-rays can be related to the absolute fission rate, if parallel plate fission chambers (4) and foils are closely attached and irradiated in the same manner. Care has to be given in this case to the particular time dependence of fission product γ-ray activity.

DESCRIPTION OF METHOD

The principle of the method is based upon the fact that ^{243}Am as well as ^{239}U decays via ^{239}Np into ^{239}Pu. So ^{239}Np is common to both decay chains and can be used to interrelate them quantitatively. The decay schemes are shown in Fig.1. The α-disintegration rate of ^{243}Am is best suited for an absolute measurement. Because of the long half life, the detection and spectrometry of the emitted α-particles can easily be performed by use of semiconductor detectors, and suitable sources can be fabricated. Therefore, it was decided to apply the low geometry α-particle counting to the absolute calibration of the ^{243}Am reference sources. This is described in detail below.

The half lives of ^{243}Am and ^{239}Np are $T_{1/2}^{53} = 7950 \pm 50$ y and $T_{1/2}^{39} = 2.35 \pm 0.01$ d, respectively. Due to the extremely long-lived parent we have the state known as secular radioactive equilibrium. And so the activity of the daughter product ^{239}Np, A^{39}, is given by

$$A^{39} = A^{53} , \qquad (1.1)$$

where $A^{39} = {}^{239}Np$ disintegration rate (sec^{-1})
$A^{53} = {}^{243}Am$ disintegration rate (sec^{-1}) .

To measure the ^{239}Np disintegration rate the 106 keV γ-x ray coincidence counting method has been chosen. By use of the ^{243}Am reference source the γ-x ray coincidence counting equipment can be calibrated precisely. For thin sources and foils, where γ-self-attenuation can be neglected, the γ-x ray coincidence counting rate of ^{239}Np, $C_{\gamma o}^{39}$, is related to the disintegration rates by

$$C_{\gamma o}^{39} = E\, A^{39} = E\, A^{53} , \qquad (1.2)$$

where E is the calibration factor.

The quantities and physical phenomena included in the calibration factor are discussed separately below. In the irradiation experiments performed, thick uranium foils were used for intensity reasons.

The measured ^{239}Np absolute disintegration rate, A^{39}, is connected to the ^{238}U capture rate, CR^{28}, by the following equation:

$$A^{39} = CR^{28}\left\{\frac{\lambda^{29}}{\lambda^{29}-\lambda^{39}}\left(1-e^{-\lambda^{39}t_i}\right)e^{-\lambda^{39}t} + \frac{\lambda^{39}}{\lambda^{39}-\lambda^{29}}\left(1-e^{-\lambda^{29}t_i}\right)e^{-\lambda^{29}t}\right\}, \quad (1.3)$$

where λ^{39}, λ^{29} = decay constants of ^{239}Np and ^{239}U, respectively

t_i = irradiation time

t = time after irradiation.

CALIBRATION OF ^{243}Am REFERENCE SOURCE

The very thin Am-source was fabricated by electroplating. The available ^{243}Am showed impurities of ^{241}Am and ^{244}Cm. By use of a high resolution semiconductor α-detector the α-peaks of ^{241}Am, ^{243}Am, and ^{244}Cm could be well separated so that the correction due to these impurities was less than 1%. To make sure that the ^{243}Am reference source was properly calibrated two independent absolute calibration methods were compared, namely the low geometry α-counting and the α-γ coincidence technique. Due to the impurities the ^{243}Am source itself has not been used for this comparison but rather a very pure ^{241}Am source prepared in the same way. Because the comparison is described elsewhere [5], only the results are given here. The absolute disintegration rate measured on the one side by low geometry α-counting and on the other side by coincidence counting agreed within 0.5 %. The total error in both determinations was estimated to be less than $\pm$ 1%.

The apparatus for the low geometry measurements is shown in Fig.2. The distance between source and surface barrier detector could be changed in discrete steps by distance holders. The aperture in front of the detector determined the solid angle. To prevent scattering from the chamber walls other apertures were inserted. Backscattering from the source backing can be neglected in this geometry as has been shown in [6]. The absolute disintegration rate of ^{241}Am, A^{51}, is given by the equation

$$A^{51} = \frac{C_\alpha}{G_s}, \quad (1.4)$$

where C_α = measured α-counting rate

G_s = geometry factor.

In the definition of (1.4) it is assumed that all α-particles impinging onto the counter are detected which is the case if semiconductor detectors are used. According to JAFFEY [7] the geometry factor G_s for a uniformly spread source coaxial with aperture is given by

$$G_s = \frac{1}{2}\left[1 - \frac{z}{\sqrt{a^2 + z^2}}\right]\left\{1 - \frac{3}{8}b^2\left[\frac{z(z + \sqrt{a^2+z^2})}{(a^2 + z^2)^2}\right]\right\} \qquad (1.5)$$

with

a = radius of aperture

b = radius of source

z = coaxial distance between source and aperture.

The second term in the curved bracket of (1.5) turned out to be negligible because of very small a/z- and b/z-ratios. In this approximation the relative error of G_s due to inaccuracies in a and z - given by $\frac{\Delta a}{a}$ and $\frac{\Delta z}{z}$ - can be found from the GAUSSIAN error propagation law by

$$\frac{\Delta G_s}{G_s} = 2\sqrt{\left(\frac{\Delta z}{z}\right)^2 + \left(\frac{\Delta a}{a}\right)^2}\,. \qquad (1.6)$$

The relative error in geometry has been estimated to be 0.007 from the relative errors $\Delta z/z = 0.002$ and $\Delta a/a = 0.003$. Other errors from α-selfabsorption in the source, backscattering effects, and electronic deadtime can be neglected. The relative statistical accuracy was always better than 0.6 %. Thus an overall error in the absolute disintegration rate of less than 1% is reliable.

DETERMINATION OF CALIBRATION FACTOR E FOR THIN SOURCES AND FOILS

In this section the calibration factor E - defined in (1.2) - is discussed, which connects the 106 keV coincidence counting rate $C^{39}_{\gamma o}$ to the absolute ^{239}Np disintegration rate A^{39}. The relation (1.2) is restricted to very thin foils in which the γ-x ray self-attenuation can be neglected. The influence of attenuation in thick foils will be considered below.

The simplicity of this calibration is evident because the detailed knowledge of all physical phenomena entering into E is not necessary. Those phenomena are due to: (a) nuclear parameters, i.e. complex decay scheme, branching ratios, electron conversion coefficients, angular correlations (γ-γ and γ-x ray), fluorescent yield, internal bremsstrahlung etc.; (b) special experimental features particular to the detecting equipment used, i.e. detector geometry, detector efficiency, source geometry, backscattering (spurious coincidences), sumcoincidences, external bremsstrahlung etc.; (c) setting of differential analyzer (window width and threshold).

Attempts to take into account all these phenomena separately fail because they are very complex and partly depend on each other. To assure that all effects are fully contained in the factor E of the relation (1.2), only three boundary conditions must be fulfilled for the ^{243}Am source and the uranium foil. Those are: (a) The layer thickness must be sufficient small so that no particles are lost due to absorption or scattering within the material. (b) The source and foil dimensions should be equal. (c) The same position between the detectors and the same setting of the electronic equipment has to be used if the source or the foil is measured.

CONSIDERATION OF γ-x RAY SELF-ATTENUATION EFFECTS IN THICK FOILS

For the actual determination of ^{238}U capture rates in fast zero power assemblies thick uranium foils have to be used for intensity reasons because only a power density of several ten milliwatts per liter is available in these systems. Appropriate foil dimensions are around 0.1 to 0.5 mm thickness and 25 mm diameter. In foils of this thickness γ-attenuation can no longer be neglected. The attenuation of the ^{239}Np 106 keV γ-x rays affects the single as well as the coincidence counting rate considerably. The effect upon the coincidence countrate is of primary interest in this context. This will be taken into account by introducing a γ-x ray selfattenuation factor S. According to its experimental determination S is defined by:

$$S = \frac{C_{\gamma}^{39}}{C_{\gamma o}^{39}} \cdot \frac{W_o}{W} \quad , \tag{1.7}$$

where $C_{\gamma o}^{39}$ = γ-x ray coincidence counting rate of a thin foil

C_{γ}^{39} = γ-x ray coincidence counting rate of a thick foil

W_o = weight of a thin foil

W = weight of a thick foil.

The experimental determination of S for a foil of thickness h is simply performed by comparing the γ-x ray coincidence counting rate of a thin reference foil to that of the thick one of equal diameter, both irradiated under the same conditions. The advantage of this procedure is that all effects depending on the foil thickness, i.e. absorption, scattering, coincidences due to backscattering, etc. are fully included in S.

A simple model has been chosen to calculate the influence of γ-x ray self-attenuation on the coincidence counting rate. The model is based on the assumption that γ ray attenuation obeys an exponential law and that γ and x-ray emission is isotropic. Furthermore, an infinite slab geometry was adopted for the foil which is a good approximation for the practical ratio of diameter to thickness. The analytical expression for S is then given by

$$S = \frac{1}{h} \int_0^h E_2(E \cdot \chi) \cdot E_2 \left[\Sigma(h - \chi)\right] \, d\chi \, , \qquad (1.8)$$

where h = thickness of foil

E_2 = second PLACZEK-integral

Σ = total macroscopic γ-scattering cross section ($16.8\ cm^{-1}$ in this case).

The factor S has been calculated as a function of h using relation (1.8). The curve is given in Fig.3. The results of experiments performed with three different foils of thickness 1.03, 14.6, and 86.0 microns are also indicated. The preparation of these uranium foils is described in [5]. It follows from Fig.3 that the agreement between experiment and calculation is quite satisfactory. As can be seen from the data even for the 1.03 microns foil, S is equal to 0.985, which means a correction of 1.5 % due to γ-x ray attenuation has to be applied. The error of S, however, is the limiting factor for the overall accuracy of about 1%. From the data a criterion can be obtained for optimum foil thickness. Assuming equal neutron irradiation

dose and uniform activation of foils with different thickness h, the coincidence counting rate C_γ^{39} is proportional to S·h. For this reason S·h versus h has been plotted in Fig.4 showing the dependence of coincidence counting rate on foil thickness. The optimum for metal foils lies around 500 microns and should be chosen if only moderate neutron doses are available.

CORRECTION DUE TO FISSION PRODUCT γ-ACTIVITY

Due to fast neutron fissions in ^{238}U - besides fissions in ^{235}U - in hard reactor spectra a considerable γ-background results from fission product activity. The corrections have to be applied for fission γ-rays falling into the 106 keV γ-x ray peak. This contribution can amount to 26% and more as shown in [8], if only single detector counting rates are investigated. This background is considerably reduced by the γ-x ray coincidence method. Results of quantitative investigations concerning the number of fission product γ-γ coincidence counts within the 106 keV peak per fission product γ-count above 1.3 MeV are given in [1]. For a ^{235}U metal foil this number is around $5 \cdot 10^{-3}$. It is assumed that this number is also true for ^{238}U.

The quantitative correction can be carried out by an experiment in which two foils of different enrichment in ^{235}U are irradiated and counted under the same conditions and if the 106 keV γ-x ray activity and γ-fission product activity above 660 keV are simultaneously measured. The arithmetical procedure is given in [5]. For foils (0.2 % ^{235}U) irradiated in a fairly hard fast reactor spectrum (Fast-Thermal Argonaut Reactor STARK, assembly 4, described in [9]) the measured correction to the ^{239}Np γ-x ray activity was less than 1%.

SET-UP OF γ-x RAY COINCIDENCE EQUIPMENT

The experimental set-up and the equipment used is shown in Fig.5. Except the stabilizing electronic circuitry the set-up and the detector design is very similar to that of TUNNICLIFFE et al. [1]. Uranium metal foils of 25.4 mm diameter and 100 micron thickness as well as the ^{243}Am-source were inserted into special foil holders (anti-Compton shields) which minimized

unwanted coincidence counts due to Compton-γ-scattering from one NaJ-crystal into the other. The crystal size was 4 inches dia. by 2 inches. RCA 7046 photomultipliers were attached to the crystals. Commercially available amplifiers, analyzers, and stabilizers (omitted in Fig.5 for simplicity) were chosen together with a coincidence unit (80 nsec time resolution) for the experiments. The complete apparatus including automatic sample changer and data acquisition system is described in detail elsewhere (10).

DISCUSSION AND CONCLUSIONS

Discussing the ^{239}Np γ-x ray coincidence method with ^{243}Am calibration in comparison to other relevant methods, several conclusions can be drawn. The potentialities of coincidence counting for ^{238}U capture rate measurements should be fully utilized to reduce the background of fission product γ-rays. In single detector γ-ray spectrometry this background is particularly cumbersome and affects the accuracy of ^{238}U capture rate measurements appreciably if foils are irradiated in fast reactor spectra. This problem has been discussed in (11) for ^{239}U disintegration rate measurements and in (8) for ^{239}Np activity determinations by single detector set-up.

Furthermore, it can be concluded that the use of ^{243}Am is essential to obtain an overall accuracy of 1% for the absolute ^{239}Np disintegration rate. This is based on the reliability of low geometry α-calibration by which any difficulty of quantitative radiochemical processing of ^{239}Np is avoided. In addition, the constant ^{243}Am-source allows a simple stability control of electronic circuitry. The main interest in precise determination of the absolute ^{238}U capture rate is its use as a reference rate for reaction rate ratios in reactor systems and in connection with ^{238}U capture cross section measurements.

2. APPLICATION OF RESONANCE ACTIVATION FOILS FOR INVESTIGATION OF NEUTRON SPECTRA IN THE keV-REGION

INTRODUCTION

The measurement of a fast reactor neutron spectrum in the low energy range from about 0.1 keV to about 100 keV is still a difficult experimental task. Although time-of-flight technique and proton-recoil proportional counters have been applied in this region to determine the differential neutron spectrum, the accuracy is still unsufficient for the comparison of theoretical and experimental results. In order to support the possiblity for intercomparing measuring techniques in this low energy range - for the elimination of systematic errors etc. - resonance absorption detectors have been investigated. Their applicability depends on various conditions: There should be only one main resonance for (n,γ)-activation in the keV-region; the (n,γ)-capture cross section, $\sigma_{n\gamma}(E)$, should be well known and large enough in the resonance and low elsewhere; the half-life of the resulting radioactive nuclei must be sufficiently long for the counting procedure, but not too long in view of the disintegration rate. Further, interfering activities from (n,p)- and (n,α)-reactions should allow either energy or half-life discrimination. Finally, the material should be suited for foil fabrication. Taking these conditions into account the nuclides ^{19}F, ^{23}Na, and ^{27}Al were chosen for investigation.

Fluorine foils were made of polytetrafluorethylene $(C_2F_4)_n$ as discs 18 mm dia. by 1.5 mm. Sodium foils were fabricated from sodium fluoride crystals with the dimensions 18 mm dia. by 1.0 mm. Aluminium was used in metallic form (18 mm dia., 0.5 mm thick). An activation analysis performed with thermal neutrons did not show any activities from impurities of the materials used.

RESONANCE PARAMETERS AND CROSS SECTIONS

The most important known resonance parameters of the three nuclides selected are given in Tab.1. The resonances of ^{19}F at energies of 15.3 and 27.3 keV found in total and capture cross section measurements are given in (12) and (13), respectively. The experimental data, particularly around the first resonance, show rather large inaccuracies so that a determination of accurate resonance parameters is not possible. Capture cross section data

for ^{19}F down to 10 keV were taken from BNL-325 (14, 15). Between 10 keV and thermal energy no measurements have been performed so far. Although in this energy region exists a superposition of contributions, the one proportional to $\frac{1}{v}$ (s-resonance) and the other proportional to v (p-resonance). A linear interpolation between thermal and 10 keV has been taken as an upper limit.

For ^{23}Na only total cross section measurements have been made around the main resonance at 2.95 keV. Therefore, the capture cross section has been calculated by J.J. SCHMIDT (16) from known resonance parameters. The calculated data have been compared to those of experiments performed above 20 keV (17) and showed good agreement.

Capture cross section measurements for ^{27}Al have been made only at thermal energy and above 20 keV so that estimations similar to ^{19}F were necessary in the intermediate range and around the 5.9 keV resonance.

For comparison of experimental and theoretical results a 26 group cross section set has been chosen for ^{19}F, ^{23}Na, and ^{27}Al. For ^{23}Na and ^{27}Al the set derived from the above mentioned microscopic cross sections is in agreement with the set of ABAGJAN et al. (18). For ^{19}F the group cross sections were made in the same way. This group cross section set for the three materials is given in Tab.2.

ACTIVATION OF RESONANCE FOILS

A thorough treatment of foil activation by neutrons under several conditions is given in (19). The results have been used to calculate corrections for the activation due to self-shielding and scattering in the resonance probes. In foils of finite thickness both effects reduce the activation by neutrons of resonance energy. Calculating the corrections, care has to be taken if the mean energy loss per collision at resonance energy is equal or smaller than the resonance width. This is the case with Na. Then, besides the probability for first collisions, also the probabilities for second, third, and fourth collisions have to be estimated and taken into account. For the example of the given Na-foil it was found that in the 2.95 keV resonance region 100 first collisions are followed by 57 to 61 further collisons (summed up to the fourth collision).

The correction factors have been applied to the group cross sections around resonance energies. For the foil dimensions, given above, the resulting group capture cross sections, $\sigma_{n\gamma_{eff}}$, computed in this way are included in Tab.2.

DECAY SCHEMES AND COUNTING METHOD

The decay and level schemes of ^{20}F, ^{24}Na, and ^{28}Al are shown in Fig.6a-c. As can be seen in all cases ß-transitions are followed by γ-deexcitations or γ-cascades, respectively. Therefore, ß-γ and γ-γ coincidence counting methods are applicable to determine absolute disintegration rates. Due to the low neutron density in fast zero power assemblies relatively thick foils have to be used; this leads to an appreciable ß-self-absorption. It was decided to count γ-rays for these reasons.

In order to calibrate the γ-counting equipment the foils were irradiated in a thermal column and their absolute disintegration rates were measured by coincidence technique. Whereas for ^{24}Na the foils of 1 mm thickness were measured directly by γ-γ coincidence method, for ^{28}Al thin foils were measured by 4π ß-γ coincidence method. Because difficulties arose with ^{20}F in the ß-γ coincidence technique due to bremsstrahlung the nuclide ^{52}V (Fig.6d), which was also measured by 4π ß-γ coincidence method, was selected additionally for calibration. By use of ^{28}Al and ^{52}V it was possible to determine the efficiency of the γ-counter at 1.78 MeV (^{28}Al) and 1.44 MeV (^{52}V). From this the efficiency for the 1.63 MeV γ-rays of ^{20}F could be interpolated.

The estimation of the total calibration error was about 2% for ^{28}Al and ^{20}F, taking into account bremsstrahlung and background, and 4% for ^{24}Na due to angular correlation, inaccuracies in the data of the complex decay schemes, sum coincidences and background.

In fast reactor irradiations primarily (n,p)- and (n,α)-reactions within the foil materials give rise to interfering activities. Reactions of the (n,2n)-type can be neglected because of their high threshold.

In case of ^{23}Na the radioactive nuclides resulting from (n,p)- and (n,α)- reactions are ^{23}Ne ($T_{1/2}$ = 38 sec) and ^{20}F ($T_{1/2}$ = 11.46 sec) with comparable short half-lives so that after a few minutes waiting time only ^{24}Na ($T_{1/2}$ = 15 h) is present.

For ^{27}Al the disturbing activities result from ^{27}Mg ($T_{1/2}$ = 9.4 min) and ^{24}Na. The γ-energies of ^{27}Mg range from 0.834 to 1.015 MeV and can be eliminated by energy discrimination. Due to its relatively long half life ^{24}Na is counted and subtracted together with the background.

Finally, in fluorine, ^{19}O ($T_{1/2}$ = 29 sec) and ^{16}N ($T_{1/2}$ = 7.15 sec) is produced besides ^{20}F. The γ-rays of ^{19}O are eliminated by energy discrimination and the upper end of the bremsstrahlungsspectrum reaching onto the photopeak

of the ^{20}F 1.63 MeV γ-line can be neglected. This is different for ^{16}N because γ-rays as well as bremsstrahlung contribute to the photopeak of ^{20}F. A correction is possible because the half-lives of ^{16}N and ^{20}F differ by a factor 1.6.

COUNTING EQUIPMENT

The irradiated foils were transported between two scintillation counters, facing each other, in order to achieve maximum efficiency. The scintillation counters themselves - consisting of 3 inches dia. by 3 inches NaI-crystals (Harshaw integral line) connected to photomultipliers (RCA 8054) - were shielded by 3 inches of lead to reduce the background from the nearby reactor. Conventional amplifiers, discriminators, and scalers were used in connection with a multichannel pulse height analyzer.

The linearity between γ-energy and pulse height was checked in the range from 0.51 MeV to 2.75 MeV using the isotopes ^{22}Na (0.51 MeV), ^{137m}Ba (0.66 MeV), ^{54}Mn (0.84 MeV), ^{65}Zn (1.12 MeV), ^{60}Co (1.33 MeV), ^{52}V (1.44 MeV), ^{28}Al (1.78 MeV), and ^{24}Na (2.75 MeV). No deviations from linearity could be observed within $\pm$ 1%. The energy resolution of the two scintillation counters at 0.66 MeV was found to be 8% and 7.8 %, respectively.

RABBIT SYSTEM

The short half lives of ^{20}F ($T_{1/2}$=11.46 sec) and ^{28}Al ($T_{1/2}$=2.28 min) require a fast transportation of the foils from the reactor. For this reason a pneumatic rabbit system was developed by which the irradiated foils were automatically placed between the detectors within 3 seconds after irradiation.

The schematic set-up of the rabbit system is shown in Fig.7. The construction of the rabbit allows an automatic mechanical opening when entering the deloading position after irradiation so that the foil is falling directly between the two detectors. The rabbit is fabricated of stainless steel with a minimum amount of material around the foil to avoid distortion of the neutron spectrum. Within the reactor the rabbit is guided by an experimental tube of 42 mm dia. fixed in an empty rectangular subassembly (2 inches by 2 inches). Foil irradiations can be performed in different axial and radial positions of the core. Outside the reactor core the guiding tube is made of plastic for maximum flexibility of the system.

The electronic control of the system is coupled to the γ-counting equipment in a way that each irradiation cycle runs preprogrammed. After loading the foil into the rabbit it will be shot into the reactor. During the preset irradiation time in the order of two or three half lives duration (40 sec for F and 5 min for Al) the γ-background is measured and stored. At the end of irradiation time the rabbit is shot back, deloads the foil into the detector station, and counting is started. The time between departure of the foil from the reactor core and start of counting is also measured in order to correct for decay. During the counting period a new foil is loaded into the rabbit, and at the end of counting the cycle starts again. The cycles were repeated until a statistical accuracy of about 1% was achieved.

Details of the mechanical construction and the electronic control system are given in (20).

CONCLUSIONS

Special results of measurements performed with F, Al, and Na in the fast core of the fast-thermal coupled Argonaut Reactor STARK are described elsewhere (9) so that here more general aspects will be discussed concerning the applicability of resonance activation detectors in fast zero power assemblies. The main conclusion from the experiments conducted so far is the verification that the foil materials investigated are fairly sensitive to changes in the low energy part of a fast reactor neutron spectrum. However, to take full advantage of this sensitivity to measure reaction rates or ratios and compare the results to those of other methods, several further improvements are necessary. This is especially important in view of resonance parameters and cross sections for ^{19}F and ^{27}Al. The partial lack of these data is the main disadvantage for the application of resonance activation detectors. Further, the perturbation of foil activation by the rabbit and its empty guiding tube inside the core have to be more thoroughly investigated. The influence of scattering and capture resonances in structural materials (Fe, Al, Na, etc.) have also to be taken into account. In combination with foils of fissible and fertile materials additional ratios of reaction rates can be measured (i.e. $^{24}Na/^{235}U$, $^{24}Na/^{238}U$, $^{20}F/^{235}U$, $^{20}F/^{28}Al$ etc.), which are a helpful tool for the investigation of spectral and heterogeneity effects in sodium and steam cooled fast reactor systems.

3. DETERMINATION OF REACTOR PARAMETERS FROM NEUTRONIC NOISE BY MEASUREMENT OF PROBABILITY DISTRIBUTIONS

INTRODUCTION

To determine the prompt neutron decay constant, the reactivity and the absolute fission rate in fast zero power assemblies several experimental techniques for reactor noise analysis have been investigated and developed in parallel. This was thought to be necessary because of the great importance of β/ℓ as integral fast reactor parameter. In large plutonium fuelled systems special consideration has to be given to the large neutron source strength from spontaneous fissions and (α,n)-reactions. For the wellknown Rossi-α technique, for example, problems arise from this because the ratio of correlated to uncorrelated detector counts decreases with increasing fission rate in the system.

The contribution of uncorrelated detector events, which is always the background in the signal, is eliminated by a new two-detector crosscorrelation method [21]. The detector output currents are passed through bandfilters, are multiplied and averaged, and the output signal, the crosspower spectral density, is free from the uncorrelated background noise. This technique has been successfully applied for measurements on STARK and also recently during the SEFOR critical experiments in ZPR III.

The method described here is based on the direct determination of probability distributions. The probabilities p_n are investigated that n processes occur in a fixed time interval of length T. A classical example is the POISSONian distribution. Its distribution law is valid for completely uncorrelated events as is the case, for instance, in radioactive decays. The existence of correlated events leads to probability distributions which deviate from the POISSONian law. The deviation is the stronger the more correlated processes are present. Reaction chains in nuclear systems and their observation by detectors are responsible for the occurence of correlated events in the detector output signals. The time behaviour of the correlated detector events is closely related to the time behaviour of the reaction chains. This is the basic reason why reactor parameters can be derived from this as well as from other noise analysis methods.

THEORY

A common theoretical basis for neutronic noise analysis experiments [22] has been used to derive formulas for the experimental technique described here. Only the results important for experimental application will be mentioned here. There are two possibilities to characterize a probability distribution: (a) by its moments, i.e. mean value, variance etc.; (b) by its probabilities p_n. Both ways will be discussed.

From the theoretical treatment of [22] only the calculation of moments is possible. In the point reactor model approximation, neglecting delayed neutrons, the equation to calculate the reactor physics parameters is given by

$$\frac{\overline{n^2}(T) - \overline{n}^2(T) - \overline{n}(T)}{T^2} = \frac{\overline{n}(T)}{T} \cdot \frac{W \gamma_2 k^2}{\alpha \ell^2} \frac{e^{-\alpha T} - 1 + \alpha T}{(\alpha T)^2} \qquad (3.1)$$

with the following symbols:

n = number of counts registered in a time interval of length T

T = length of a time interval

W = detector efficiency

k = multiplication constant

ℓ = prompt neutron lifetime

$\gamma_2 = \frac{\overline{\nu(\nu-1)}}{\overline{\nu}^2}$ = nuclear parameter

ν = number of neutrons per fission

β = effective fraction of delayed neutrons

$\alpha = \frac{1 - k_p}{\ell} = \frac{1-k(1-\beta)}{\ell}$ = prompt neutron decay constant.

The numerator on the left hand side of (3.1) contains the difference between the measured variance $(\overline{n^2} - \overline{n}^2)$ and the variance of the POISSON distribution which is equal to $\overline{n}$. A rearrangement of (3.1) leads to the equivalent formulation

$$\frac{\overline{n(n-1)}\,(T) - \overline{n}^2(T)}{\overline{n}(T)} = W \gamma_2 \frac{k^2}{(1-k_p)^2} \left[1 - \frac{1 - e^{-\alpha T}}{\alpha T} \right], \qquad (3.2)$$

which has been used for the evaluation of the experimental results. This expression gives the deviation from the reduced variance (normal variance divided by mean value) of the POISSON distribution and results solely from correlated detector events. The uncorrelated background noise is, therefore, already eliminated. Eq.(3.2) consists of two distinct terms on the right hand side. The second one within the brackets represents the mean time behaviour of correlated processes. It approaches unity for $T \longrightarrow \infty$. In this case the time interval of observation is so long that all correlations of detector events have been taken into account. The first term contains the dependence on detector efficiency, reactivity, and nuclear constants. Near the delayed critical state it is

$$\left(\frac{\overline{n(n-1)} - \bar{n}^2}{\bar{n}} \right)_{T \longrightarrow \infty} = W \gamma_2 \frac{k^2}{(1-k_p)^2} = W \frac{\gamma_2}{\beta^2} \left[\frac{\alpha_c}{\alpha} \right]^2 . \qquad (3.3)$$

The efficiency W can be calculated from (3.3) if $\alpha_c = \beta/\ell$ and α have been determined from the measurements and if β is known from reactor calculations. The absolute fission rate F in the system is given by

$$F = \frac{C}{W} , \qquad (3.4)$$

where C is the mean counting rate in the experiment. The reactivity follows from the relation

$$-\rho \left[\$ \right] = \frac{\alpha}{\alpha_c} - 1 . \qquad (3.5)$$

The second way, the direct calculation of probabilities $p_n(T)$ has been investigated by ZOLOTUKHIN and MOGILNER [23]. They used the technique of probability generating functions to calculate the distributions. The probability generating function E(T,u) is defined by

$$E(T,u) = \sum_{n=o}^{\infty} p_n(T)\, u^n , \qquad (3.6)$$

where T = length of a time interval

u = auxiliary variable.

The main purpose for the introduction of a probability generating function is an easy computation of probabilities and moments. From (3.6) follows:

$$p_n = \frac{1}{n!} \left. \frac{d^n E(T,u)}{du^n} \right|_{u=0} , \tag{3.7}$$

$$\text{variance} = \left. \frac{d^2 E(T,u)}{du^2} \right|_{u=1} + \left. \frac{dE(T,u)}{du} \right|_{u=1} - \left\{ \left. \frac{dE(T,u)}{du} \right|_{u=1} \right\}^2 . \tag{3.8}$$

In the point reactor model approximation and neglecting delayed neutrons the probability generating function of ZOLOTUKHIN and MOGILNER [23] is given by

$$\ln E(T,u) = \bar{n}(T)(u-1) \left\{ \frac{1-\varphi}{\hat{z}(u-1)} - \frac{2}{\alpha T \hat{z}(u-1)} \ln \left[1 + \frac{(\varphi-1)^2}{4\varphi} \left(1-e^{-\alpha T \varphi}\right) \right] \right\} , \tag{3.9}$$

where

$$\varphi = \sqrt{1 - 2\hat{z}(u-1)} \tag{3.9a}$$

$$\hat{z} = \frac{W \cdot \chi_2 \, k^2}{(1-k_p)^2} \tag{3.9b}$$

with the symbols already defined. The probabilities p_n can principally be derived from (3.9) using relation (3.7). The probability p_o, that nothing is registered during the time interval T, follows as

$$p_o(T) = e^{-\bar{n}(T) \frac{2}{\varphi_o+1} \left\{ 1 + \frac{2}{(\varphi_o-1)\alpha T} \ln \left[1 + \frac{(\varphi_o-1)^2}{4\varphi_o} \left(1-e^{-\alpha T \varphi_o}\right) \right] \right\}} \tag{3.10}$$

with

$$\varphi(\hat{z}, u=0) = \varphi_o = \sqrt{1 + 2\hat{z}} .$$

If p_o and $\bar{n}$ are measured for different values of T the parameters α, k, and W can be found. The computation of probabilities with higher values of n, however, is merely impossible in this manner. For the limiting case $\alpha T \longrightarrow \infty$ the probability generating function (3.9) reduces to

$$E_{\infty}(u) = e^{\frac{\bar{n}}{\hat{z}} \left(1 - \sqrt{1 - 2\hat{z}(u-1)}\right)} \tag{3.11}$$

By use of (3.7) and repeated differentiation the following recursion formula can be set up:

$$p_{n\infty} = p_{m+i} = \frac{\bar{n}}{(1+m)\sqrt{1+2\hat{z}}} \sum_{j=0}^{m} p_{m-j} \frac{(2j-1)!!}{j!} \left[\frac{\hat{z}}{1+2\hat{z}}\right]^j . \qquad (3.12)$$

The reduced variance was also computed by use of (3.8) to compare the results of both theoretical ways. The expression found was identical to (3.1).

The connection between the distribution of probabilities p_n and the mean value, variance, etc. is given by the following relations:

$$\bar{n}(T) = \sum_{n=1}^{\infty} p_n(T)\, n \qquad (3.13)$$

$$\overline{n^2}(T) = \sum_{n=1}^{\infty} p_n(T)\, n^2 \qquad (3.14)$$

$$\overline{n(n-1)}\,(T) - \bar{n}^2(T) = \sum_{n=2}^{\infty} p_n(T)\, n(n-1) - \left[\sum_{n=1}^{\infty} p_n(T)\, n\right]^2 . \qquad (3.15)$$

In our method the probabilities $p_n(T)$ are determined for different values of T by the "probability distribution analyzer", described below. From the p_n the left hand side of (3.2) is computed by use of relations (3.13) to (3.15). By fitting the expression (3.2) to the experimental curves the reactor parameters can be derived.

PROBABILITY DISTRIBUTION ANALYZER

An experimental set-up was built for the direct measurement of the probabilities $p_n(T)$, where n can range from 0 to 127. This probability distribution analyzer is schematically shown in Fig.8. The operating principle is as follows: Pulses from one or more detectors are fed into the input A of a fast acting electronic step switch, which proceeds by one step for each incoming pulse. Pulses from a time marker terminating the length T of the time interval are fed into input B. According to the position of the electronic switch, a gate is opened for the time pulse which gives a signal to the scaler connected to this output. If, for instance, 4 counts came in during the interval, output 4 of the switch opens gate 4 so that the pulse from the time marker delivers a signal into scaler 4. That means, that 4 counts came in during this time interval. The step switch is reset and the probability distribution analyzer is opened for a new cycle. After a sufficiently long time the run

for one T-value is finished and the probabilities $p_n(T)$ are obtained directly by dividing the number of counts in scaler n, R_n , by the number of counts in the time interval scaler, R_T , giving

$$p_n = \frac{R_n}{R_T} \quad . \tag{3.16}$$

The performance of the analyzer is checked by the monitor scaler, because the relation

$$R_D = \sum_{n=1}^{127} n R_n \tag{3.17}$$

must be satisfied for the number of counts in the monitor scaler, R_D . An additional check is given by

$$R_T = \sum_{n=0}^{127} R_n \quad . \tag{3.18}$$

The analyzer was designed for high counting rates (20 Mc per sec), a necessity for experiments in plutonium-fuelled fast assemblies. Therefore, a large number of detector counts can be handled in relatively short measuring times according to the statistical accuracy required. Because many measurements have to be performed in a variety of reactor assemblies automatic components are built into the experimental set-up. The complete data acquisition and reduction system is shown in Fig.9. By means of a tape reader a sequence of T-values, repetitive or successive, are given into the time marker. Within the range from 10 µsec to 640 msec 51 time interval lengths may be chosen in discrete steps. This is sufficient for measurements in fast and thermal systems.

An experiment is usually run in the following way: According to the assembly investigated and its state of reactivity the sequence, magnitudes, and number of time interval lengths are programmed. Usually one T-value is repeated several times in order to see and to exclude drift effects of the reactor or electronics. The measuring time per interval length depends on the counting rate and the statistical accuracy required. For each value of T (and its repetitions) the complete probability distribution is measured. If the run is finished the scaler outputs are punched on tape and written out for control before the next run is started. All data of the experiment are collected and fed into an electronic computer for evaluation according to relations (3.13) to (3.15) and (3.2). A least squares fit is used to derive the prompt neutron decay constant and the quantity $\hat{z}$ given by (3.3) and (3.9b), respectively.

RESULTS

Measurements have been performed on the fast-thermal Argonaut Reactor STARK [9] from which a few typical results shall be discussed here for further explanation of the technique. In Fig.10 measured probability distributions (full line) are shown for five different values of the time interval length T. In addition, equivalent POISSON distributions (dashed line) are included for comparison. The distributions are taken from an experiment where high detector efficiency was available. The quantity $\hat{z}$, which gives the maximum ratio of correlated to uncorrelated detector events, was 1.64 and α was 139 sec^{-1}. Due to the large $\hat{z}$-values the deviation from the POISSONian law is clearly visible, increasing with larger values of T. For very large T ($T \longrightarrow \infty$) the asymptotic probability distribution was measured during another experiment and evaluated by use of relation (3.12). The reactor parameters derived agreed very well to those found by other means.

The normal way of evaluation, however, is done by use of (3.2). An example for the experimentally determined deviation from the reduced variance of the POISSON distribution as function of interval length T is shown in Fig.11. In this experiment the detector efficiency was much lower and, therefore, $\hat{z}$ was 0.34, which means that only 34% (maximum) of correlated events were present in the detector output signals. At least 10^5 detector counts were analyzed per T-value indicated in the curve of Fig.11. Other experiments were conducted on STARK under various conditions to determine the range in which the method of probability distribution analysis can be applied successfully.

CONCLUSIONS

The most important conclusion from the experiments performed on STARK is that even $\hat{z}$-values around 0.3 allow an accurate (ca. 2 - 3%) determination of the prompt neutron decay constant α by this method. On the basis of this result all necessary data for the application in plutonium-fuelled fast assemblies can be estimated. This has been done, and the results are listed in Tab.3. A fast reactor assembly with 300 kg Pu (92% ^{239}Pu, 8% ^{240}Pu) was chosen. The data used for computation are: Neutron source strength due to spontaneous fissions and (α,n)-reactions $s_o = 3 \cdot 10^7$ neutrons per sec, prompt neutron decay constant at delayed critical $\alpha_c = 6.7 \cdot 10^3$ sec^{-1}, effective fraction of delayed

neutron, $\beta = 3.5 \cdot 10^{-3}$, and the nuclear parameter $\gamma_2 = 0.8$. With the constant value $\hat{z} = 0.35$ the following quantities have been calculated in the reactivity range from 0.1 to 4 dollars: Fission rate F in the system, reactor power P, minimum detector efficiency W, mean detector counting rate ξ, order of magnitude for time interval length T, and mean value of detector counts per interval $\bar{n}$. As can be seen from the estimated results measurements of α can be conducted between reactivities of ca. 0.2 and 3 dollars. No measurement is possible at delayed critical due to the relatively large power. The prompt neutron decay constant at delayed critical has, therefore, to be determined by extrapolation. Because of the high counting rates the time necessary for the measurement of one α-value should not exceed 20 minutes. Finally, it can be concluded that the technique of probability distribution analysis is applicable to determine reactor physics parameters in fast uranium and plutonium fuelled reactor assemblies.

REFERENCES

(1) P.R. TUNNICLIFFE, D.J. SKILLINGS, B.G. CHIDLEY, "A Method for the Accurate Determination of Relative Initial Conversion Ratios", Nucl. Sci. and Eng. 15, 268 (1963)

(2) R. SHER, "γ-γ Coincidence Method for Measuring Resonance Escape Probability in ^{238}U Lattices", Nucl. Sci. and Eng. 7, 479 (1960)

(3) A. WEITZBERG and T.J. THOMPSON, "Coincidence Technique for ^{238}U Activation Measurements", Trans. Am. Nucl. Soc. 3, 456 (1960)

(4) F.S. KIRN, "Neutron Detection with an Absolute Fission Counter", Proc. Symp. on Neutron Detection, Dosimetry, and Standardization, sponsored by IAEA, Harwell, Vol.II, p.497 (1963)

(5) H.SEUFERT and D.STEGEMANN, "A Method for Absolute Determination of ^{238}U-Capture Rates in Fast Zero Power Reactors", Nucl. Sci. and Eng., in press

(6) D.H. WALKER, "An Experimental Study of the Backscattering of 5.3 MeV Alpha Particles from Platinum and Monel Metal", Intern. Journal Appl. Rad. and Isotopes 16, 183 (1965)

(7) A.H. JAFFEY, "Solid Angle Subtended by a Circular Aperture at Point and Spread Sources", Rev. Scient. Instr. 25, 349 (1954)

(8) R.R. SMITH et al., "The Breeding Ratio of a Plutonium Loading in EBR-I", ANL-6789, Argonne National Laboratory (1964)

(9) L. BARLEON et al., "Evaluation of Reactor Physics Experiments on the Coupled Fast-Thermal Argonaut Reactor STARK", Paper presented at this Conference

(10) K.H. BLANK and H. SEUFERT, "An Automatic Sample Changer with a Special Changing Method for γ- and γ-γ-Active Sources, Nucl. Instr. and Methods, in press

(11) W.G. DAVEY, "The Ratio of ^{238}U Capture and ^{235}U Fission Cross Sections in Fast Reactors", Nucl. Sci. and Eng. 24, 26 (1966)

(12) C.T. HIBDON, "Nuclear Levels of F^{20}", Phys. Rev. 133, No 2 B, 353 (1964)

(13) R.L. MACKLIN et al., "Neutron Capture Cross Sections near 30 keV Using a Moxon-Rae Detector", Nucl. Phys. 43, 353 (1963)

(14) D.J. HUGHES et al., "Neutron Cross Sections", BNL-325, Suppl.No.1, Brookhaven National Laboratory (1960)

(15) J.R. STEHN et al., "Neutron Cross Sections", BNL-325, Suppl.No.2, Brookhaven National Laboratory (1964)

(16) J.J. SCHMIDT, "Neutron Cross Sections for Fast Reactor Materials", KFK-120, Kernforschungszentrum Karlsruhe (1962)

(17) S.J. BAME et al., "(n,γ) Cross Sections of Na^{23}, I^{127}, and Au^{197}", Phys. Rev. 113, No 1, 256 (1959)

(18) L.P. ABAGJAN, N.O. BAZAZJANC, I.I. BONDARENKO, M.N. NIKOLAEV, "Gruppenkonstanten schneller und intermediärer Neutronen für die Berechnung von Kernreaktoren", KFK-tr-144, Translation of Kernforschungszentrum Karlsruhe (1964)

(19) K.H. BECKURTS, K. WIRTZ, "Neutron Physics", Chapter 11 and 12, Springer Verlag (1964)

(20) W. BACKFISCH, A. BAYER, "Eine vollautomatische Rohrpostanlage zur Bestrahlung und Auszählung kurzlebiger Aktivierungssonden", to be published

(21) W. SEIFRITZ, D. STEGEMANN, W. VÄTH, "Two-Detector Crosscorrelation Experiments in the Fast-Thermal Argonaut Reactor STARK", Proc. of the Int. Symp. on Neutron Noise, Wave, and Pulse Propagation, Gainesville, Florida (1966) and KFK-413, Kernforschungszentrum Karlsruhe (1966)

(22) H. BORGWALDT, D. STEGEMANN, "A Common Theory for Neutronic Noise Analysis Experiments in Nuclear Reactors, Nukleonik 7, 313 (1965)

(23) V.G. ZOLOTUKHIN, A.J. MOGILNER, "The Distribution of Neutron Counts from a Detector Placed in a Reactor", Atomnaya Energia 15, 11 (1963).

LIST OF TABLES AND FIGURES

TAB.1 Resonance Parameters for ^{19}F, ^{23}Na, and ^{27}Al

Nucleus	I^{π}	E_o	Γ	Γ_n	Γ_γ	ℓ	J^{π}	$\Gamma_{Doppler}$
^{19}F	$^1/_2{}^+$	15.3 keV						9 eV
		27.3 keV	0.3 keV		0.7±0.2 eV	1	2^-	12 eV
^{23}Na	$^3/_2{}^+$	2.95 keV	0.2204 keV	0.22 keV	0.4 eV	0	2	3.6 eV
		54.1 keV		0.75 keV		1	3	} 15.5 eV
		55 keV		0.20 keV		0	2	
^{27}Al	$^5/_2{}^+$	5.906 keV	0.02 keV			1		4.7 eV
		35.04 keV				0	3	11.8 eV

TAB.2 Group Cross Sections for ^{19}F, ^{23}Na, and ^{27}Al

		^{19}F		^{23}Na				^{27}Al		
i	E_n	$\sigma_{n\gamma}$	$\sigma_{n\gamma_{eff}}$	σ_t	$\sigma_{n\gamma}$	$\sigma_{n\gamma_{eff}}$	U	σ_t	$\sigma_{n\gamma}$	$\sigma_{n\gamma_{eff}}$
1	6.5 - 10.5 MeV	0.00002		2.20	0.00015 +)		0.48	1.90	0.0002 +)	
2	4.0 - 6.5 MeV	0.00002		2.30	0.00015 +)		0.48	2.20	0.0002 +)	
3	2.5 - 4.0 MeV	0.00004		2.60	0.0001 +)		0.48	2.70	0.0004 +)	
4	1.4 - 2.5 MeV	0.00012		3.00	0.00015 +)		0.57	3.00	0.0004	
5	0.8 - 1.4 MeV	0.00018		3.80	0.0002		0.57	3.20	0.0004	
6	0.4 - 0.8 MeV	0.00045		4.50	0.0003		0.69	4.00	0.0007	
7	0.2 - 0.4 MeV	0.0005		4.00	0.0006		0.69	3.90	0.001	
8	0.1 - 0.2 MeV	0.0006		3.80	0.0012		0.69	5.20	0.003	
9	46.5 -100 keV	0.0020	0.0015	5.30	0.0016		0.77	5.00	0.002	
10	21.5 - 46.5 keV	0.0075	0.0051	4.30	0.0026		0.77	7.40	0.006	0.0055
11	10.0 - 21.5 keV	0.0050	0.0047	5.00	0.001		0.77	1.00	0.001	
12	4.65- 10.0 keV	0.0035		8.00	0.001		0.77	2.60	0.060	0.052
13	2.15- 4.65 keV	0.0036		100.1	0.060	0.043	0.77	1.40	0.0007	
14	1.0 - 2.15 keV	0.0038		6.21	0.010		0.77	1.40	0.0010	
15	465 -1000 eV	0.004		3.30	0.005		0.77	1.40	0.0015	
16	215 -465 eV	0.0042		3.11	0.006		0.77	1.40	0.0021	
17	100 -215 eV	0.0045		3.11	0.007		0.77	1.40	0.0031	
18	46.5 -100 eV	0.005		3.11	0.010		0.77	1.40	0.0046	
19	21.5 - 46,5 eV	0.005		3.12	0.015		0.77	1.41	0.0067	
20	10.0 - 21.5 eV	0.0055		3.12	0.022		0.77	1.41	0.010	
21	4.65- 10 eV	0.006		3.13	0.032		0.77	1.42	0.015	
22	2.15- 4.65 eV	0.006		3.15	0.046		0.77	1.42	0.021	
23	1.0 - 2.15 eV	0.0065		3.17	0.068		0.77	1.43	0.031	
24	0.465- 1.0 eV	0.007		3.20	0.101		0.77	1.45	0.046	
25	0.215- 0.465 eV	0.0075		3.25	0.147		0.77	1.47	0.067	
T	0.0252 0.009	0.009		3.63	0.525			1.64	0.241	
					0.465					

+) Corrected values: In the original work the $\sigma_{n\alpha}$ and σ_{np} cross sections are enclosed.

TAB.3 Estimated Data for Application of Probability Distribution Analysis in Fast Plutonium Fuelled Reactor Assemblies

$-\rho(\$)$	F (sec^{-1})	P(W)	W	$\xi\,(sec^{-1})$	$T = \frac{1}{\alpha}$ (sec)	$\bar{n}$
0.1	$3.12 \cdot 10^{10}$	$9.8 \cdot 10^{-1}$	$6.5 \cdot 10^{-6}$	$2.0 \cdot 10^{5}$	$1.35 \cdot 10^{-4}$	27.3
0.2	$1.56 \cdot 10^{10}$	$4.9 \cdot 10^{-1}$	$7.7 \cdot 10^{-6}$	$1.2 \cdot 10^{5}$	$1.24 \cdot 10^{-4}$	14.9
0.3	$1.04 \cdot 10^{10}$	$3.3 \cdot 10^{-1}$	$9.1 \cdot 10^{-6}$	$9.4 \cdot 10^{4}$	$1.15 \cdot 10^{-4}$	10.8
0.4	$7.80 \cdot 10^{9}$	$2.4 \cdot 10^{-1}$	$1.1 \cdot 10^{-5}$	$8.2 \cdot 10^{4}$	$1.07 \cdot 10^{-4}$	8.7
0.5	$6.25 \cdot 10^{9}$	$2.0 \cdot 10^{-1}$	$1.2 \cdot 10^{-5}$	$7.5 \cdot 10^{4}$	$9.95 \cdot 10^{-5}$	7.5
0.7	$4.45 \cdot 10^{9}$	$1.4 \cdot 10^{-1}$	$1.6 \cdot 10^{-5}$	$6.9 \cdot 10^{4}$	$8.78 \cdot 10^{-5}$	6.1
1.0	$3.12 \cdot 10^{9}$	$9.8 \cdot 10^{-2}$	$2.1 \cdot 10^{-5}$	$6.7 \cdot 10^{4}$	$7.45 \cdot 10^{-5}$	5.0
1.5	$2.08 \cdot 10^{9}$	$6.5 \cdot 10^{-2}$	$3.3 \cdot 10^{-5}$	$6.9 \cdot 10^{4}$	$5.97 \cdot 10^{-5}$	4.1
2.0	$1.56 \cdot 10^{9}$	$4.9 \cdot 10^{-2}$	$4.8 \cdot 10^{-5}$	$7.5 \cdot 10^{4}$	$4.97 \cdot 10^{-5}$	3.7
2.5	$1.25 \cdot 10^{9}$	$3.9 \cdot 10^{-2}$	$6.5 \cdot 10^{-5}$	$8.1 \cdot 10^{4}$	$4.28 \cdot 10^{-5}$	3.5
3.0	$1.04 \cdot 10^{9}$	$3.3 \cdot 10^{-2}$	$8.6 \cdot 10^{-5}$	$8.9 \cdot 10^{4}$	$3.73 \cdot 10^{-5}$	3.3
3.5	$8.91 \cdot 10^{9}$	$2.8 \cdot 10^{-2}$	$1.1 \cdot 10^{-4}$	$9.6 \cdot 10^{4}$	$3.02 \cdot 10^{-5}$	2.9
4.0	$7.80 \cdot 10^{8}$	$2.4 \cdot 10^{-2}$	$1.3 \cdot 10^{-4}$	$1.0 \cdot 10^{5}$	$2.98 \cdot 10^{-5}$	3.0

Values used for calculation: $\hat{z} = 0.35$; $\chi_2 = 0.8$; $\beta = 3.5 \cdot 10^{-3}$

$s_o = 3 \cdot 10^{7}\ sec^{-1}$; $\alpha_c = 6.7 \cdot 10^{3}\ sec^{-1}$.

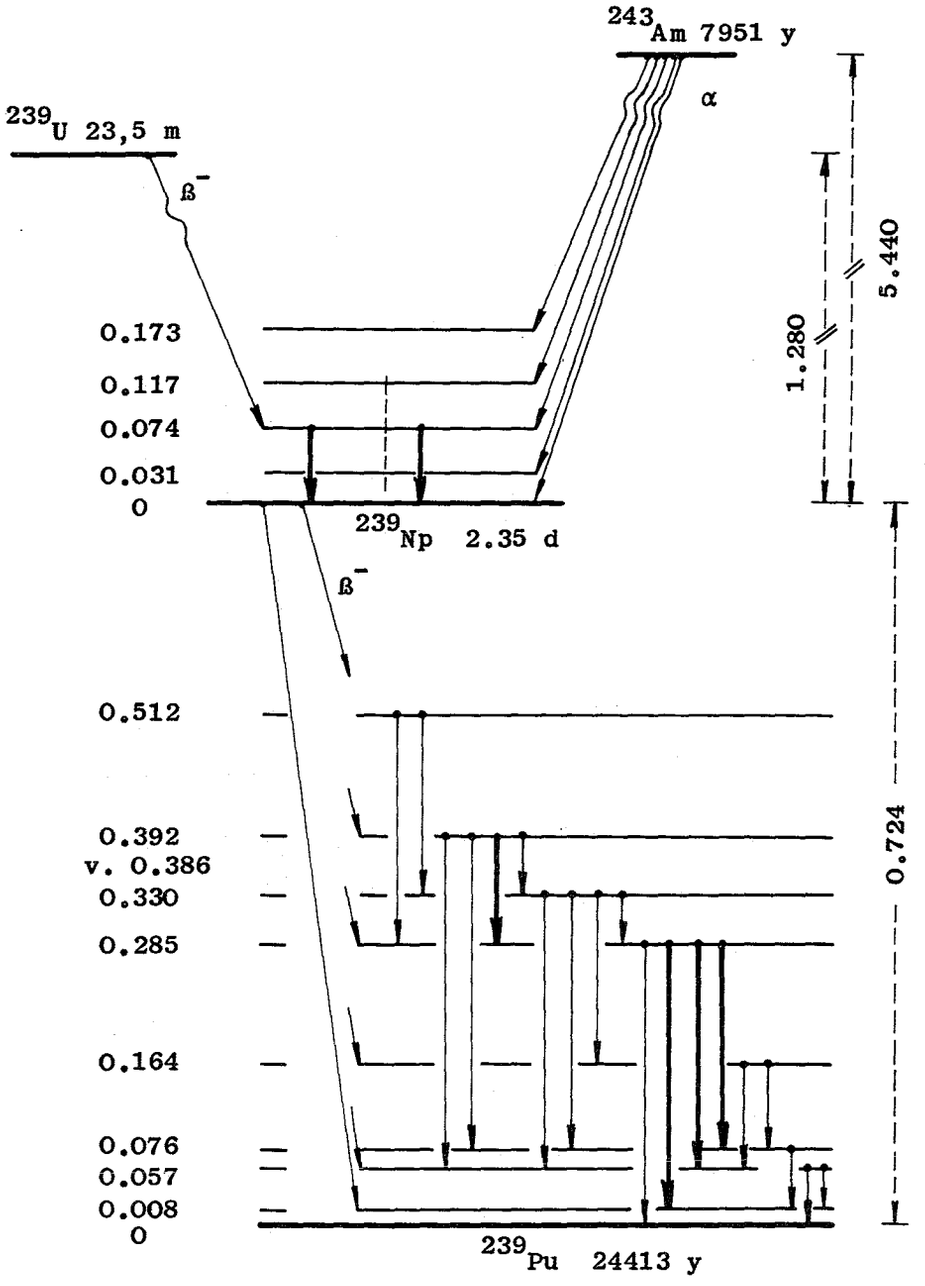

FIG.1 Combined decay schemes

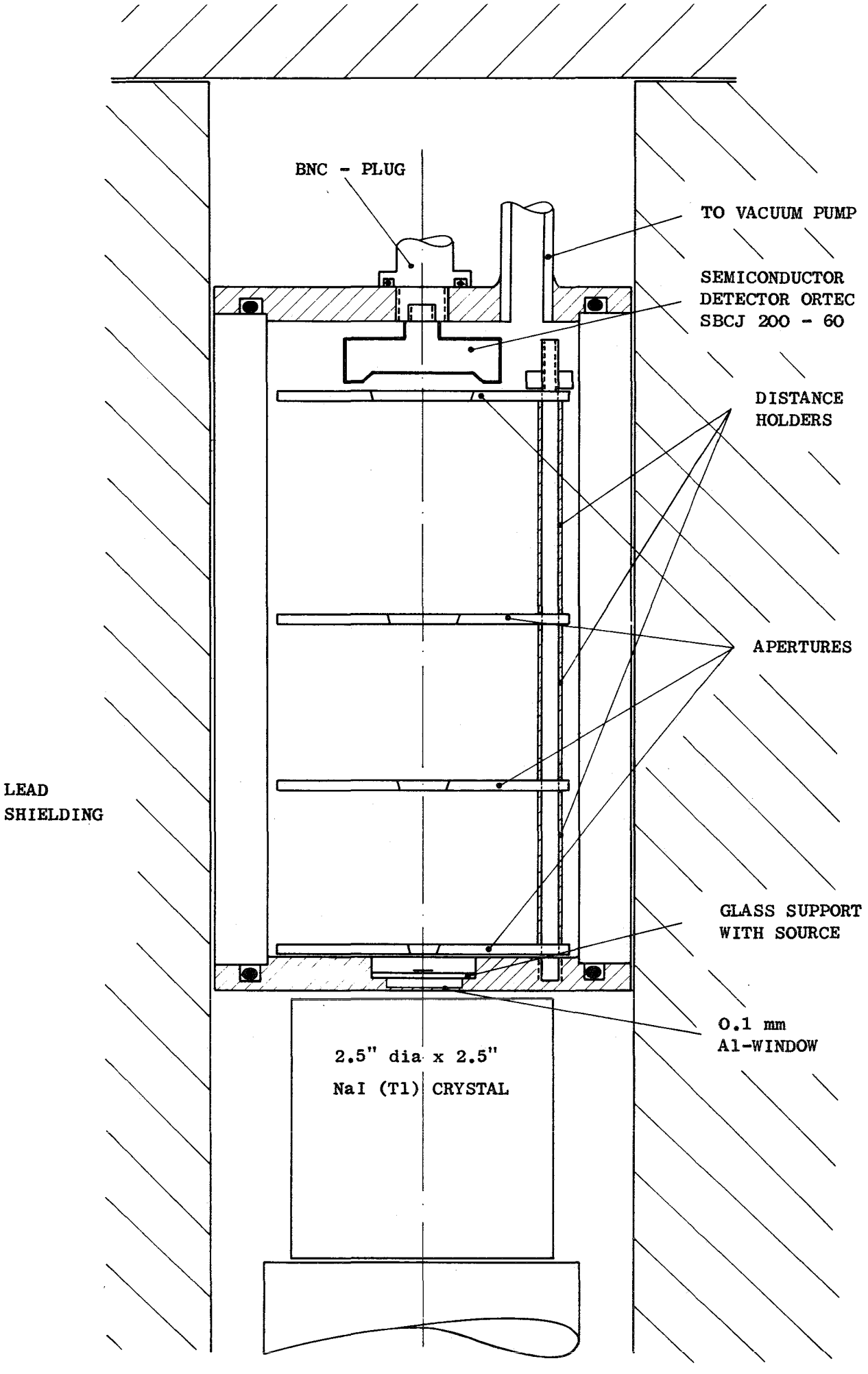

FIG.2 Apparatus for α and α-γ calibration

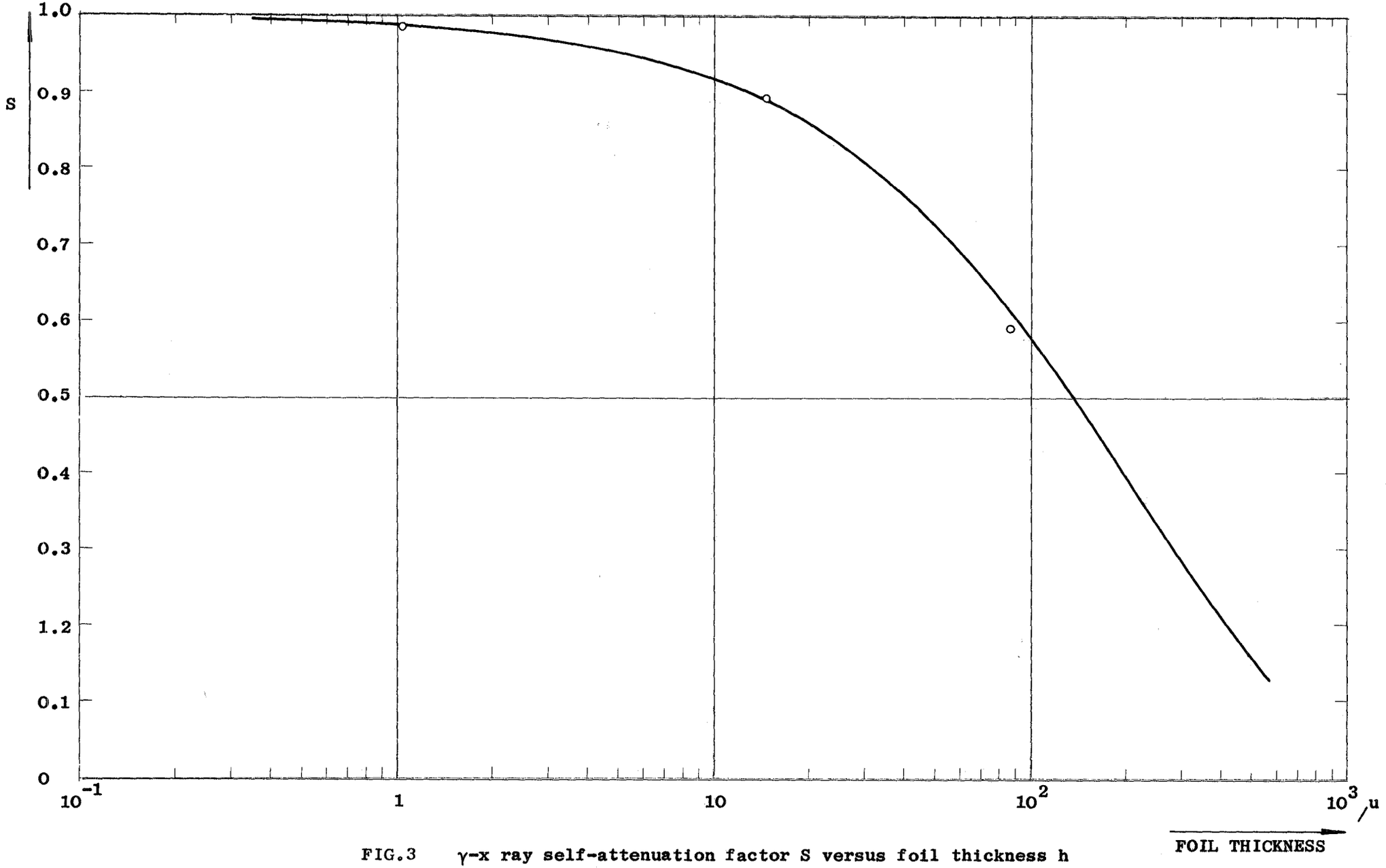

FIG.3 γ-x ray self-attenuation factor S versus foil thickness h

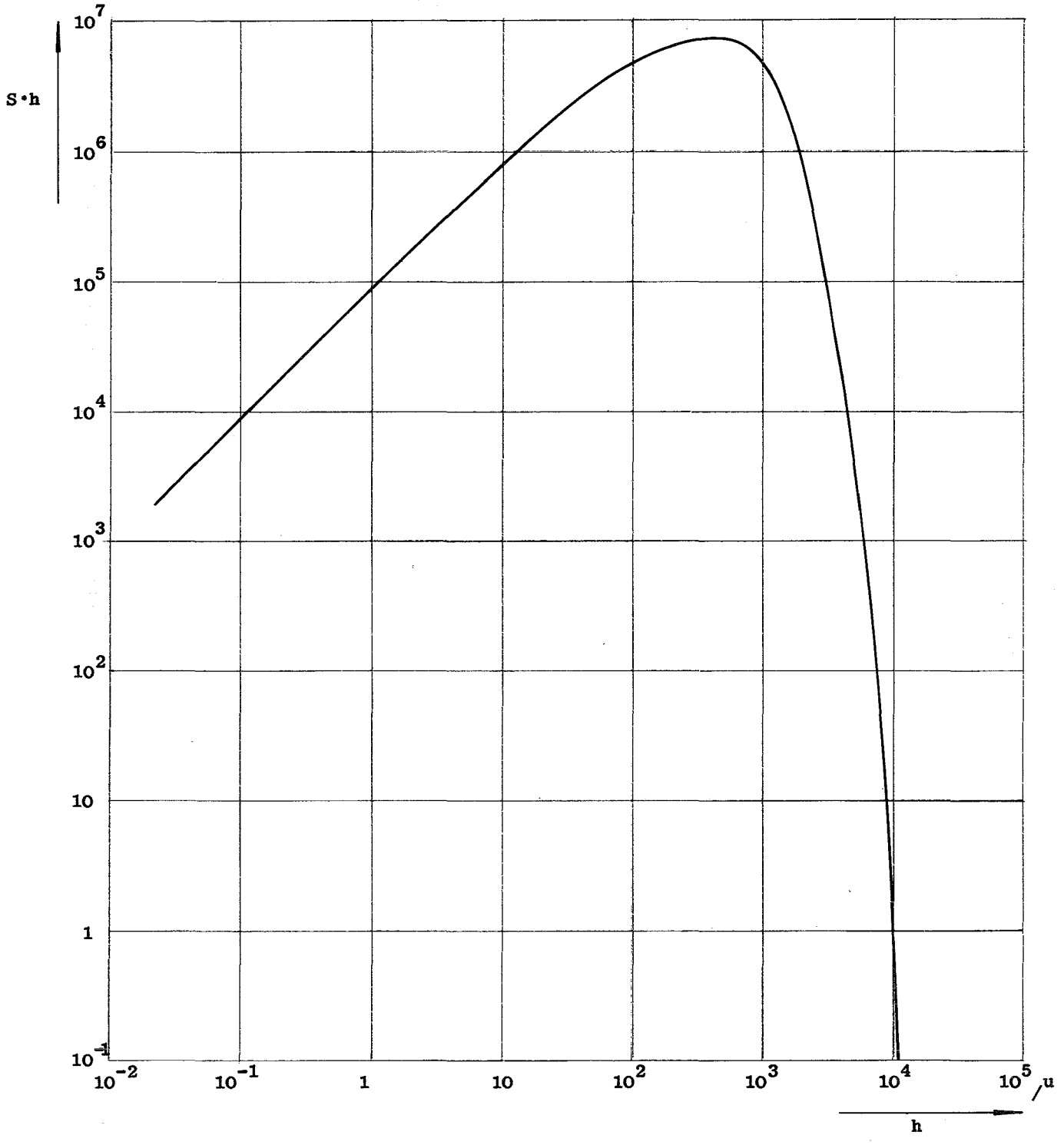

FIG.4 S•h versus h

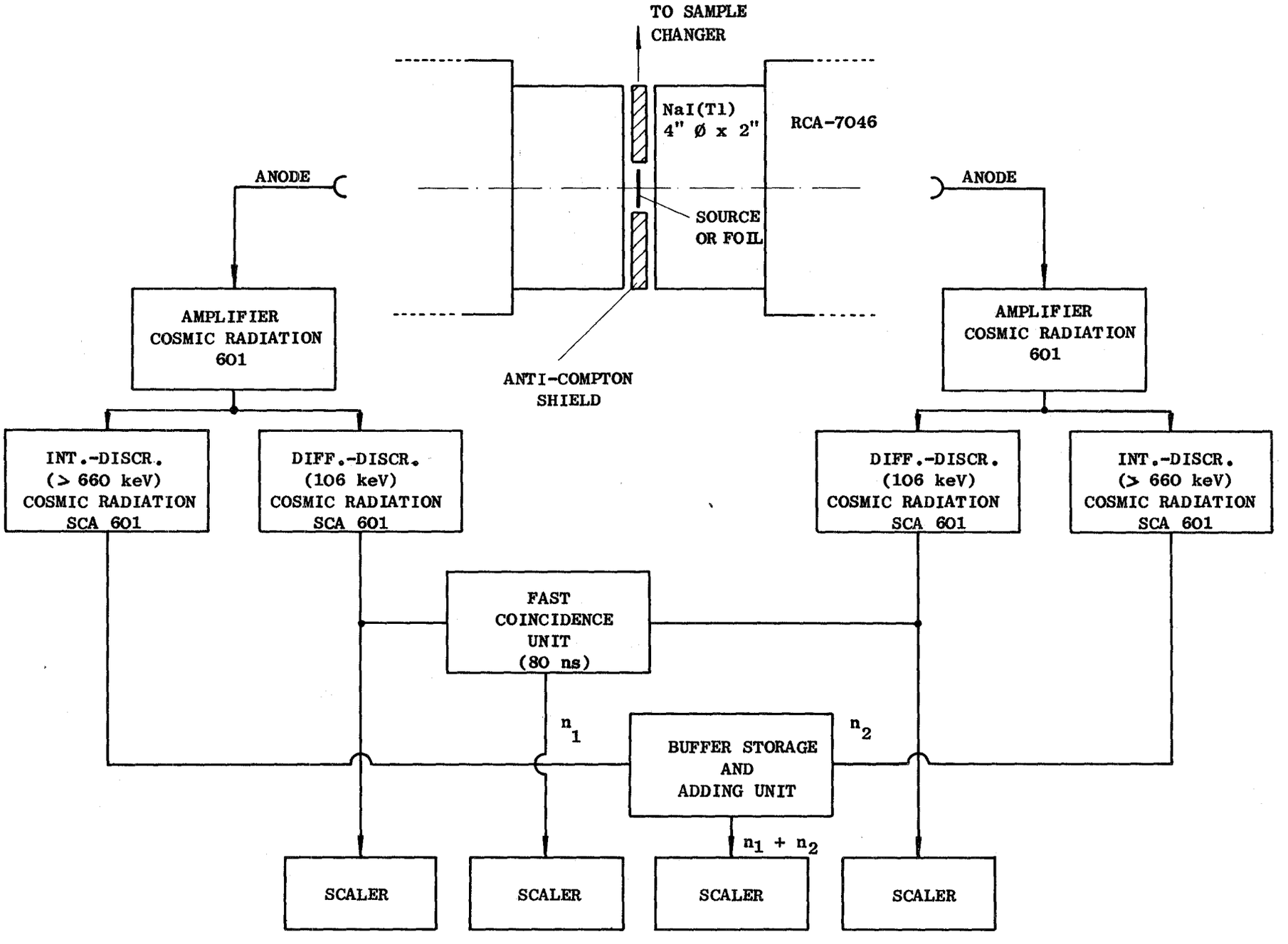

FIG.5 Set-up of γ-x ray coincidence equipment

Fig. 6 : Decay Schemes of ^{20}F, ^{24}Na, ^{28}Al and ^{52}V

Fig. 6a : F 20

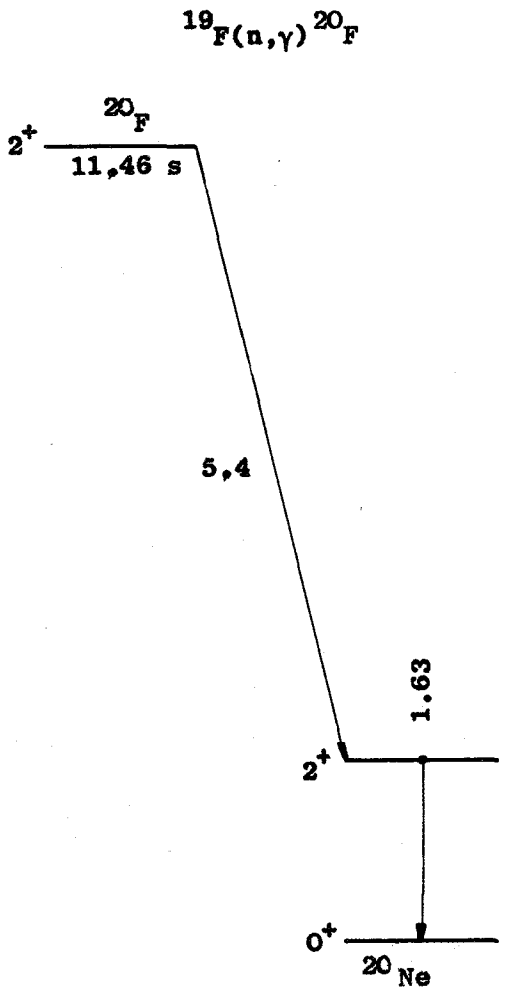

Fig. 6b : Na 24

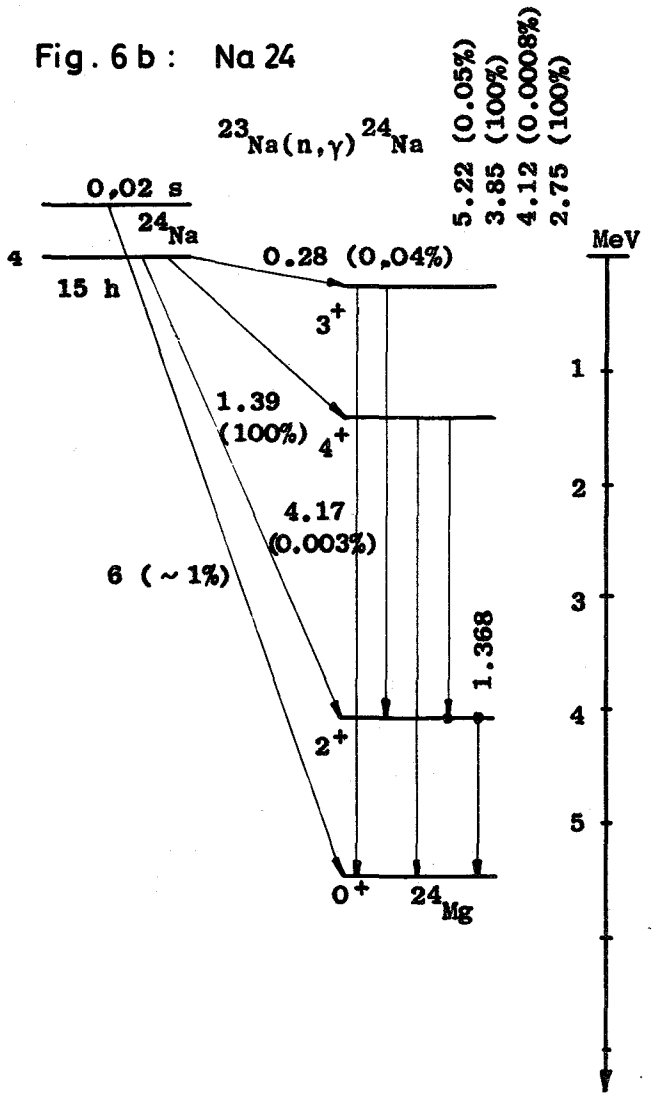

Fig. 6c : Al 28

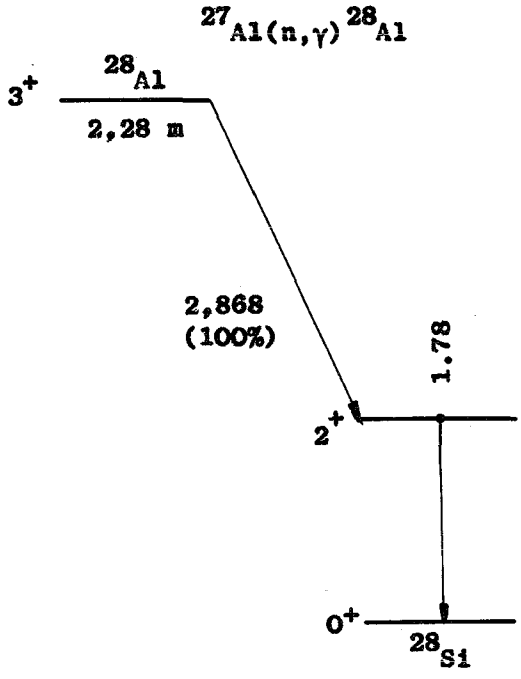

Fig. 6d : V 52

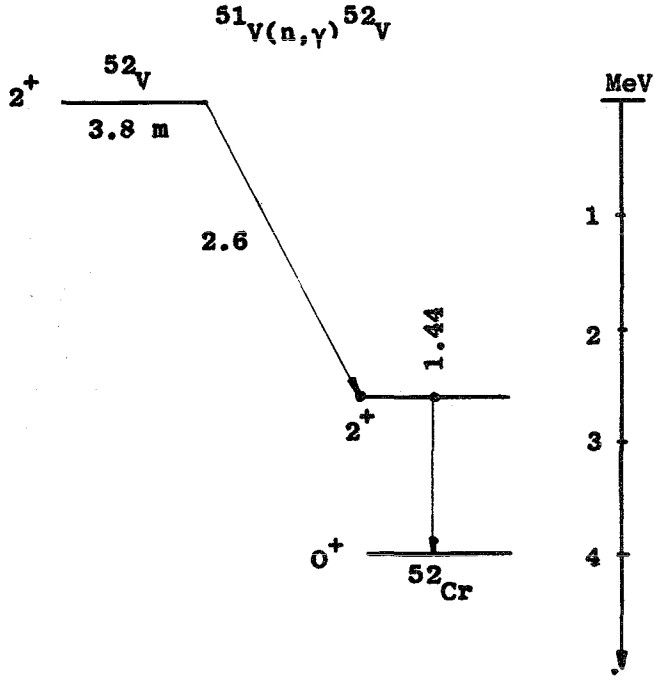

Fig.7 : Set-up of Rabbit-System

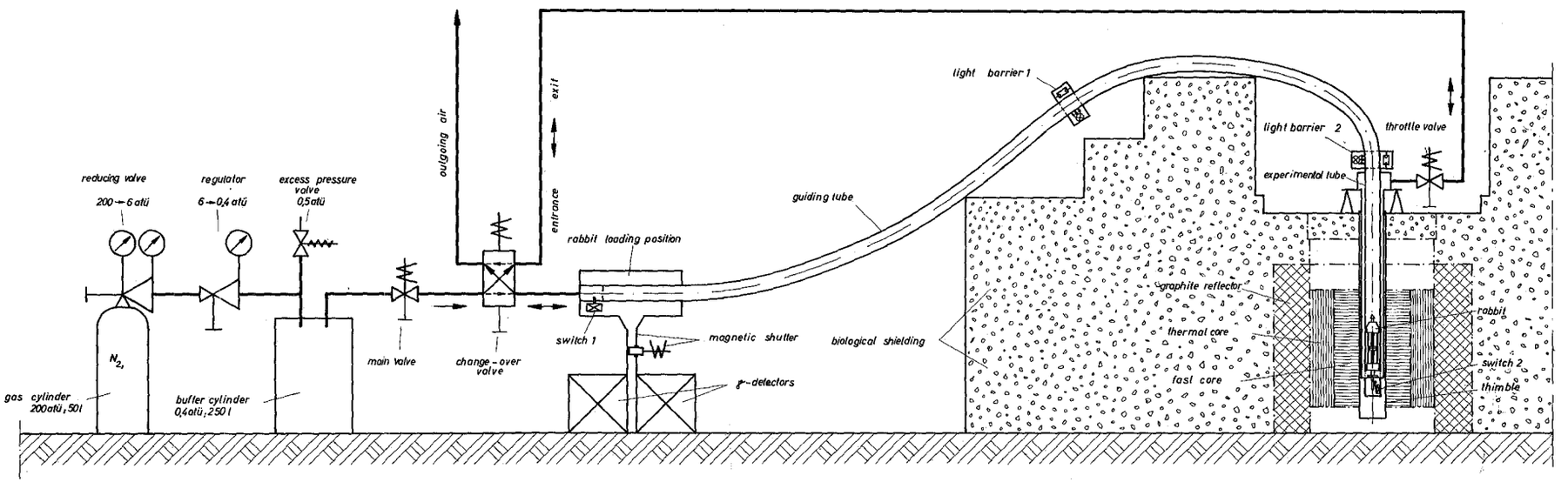

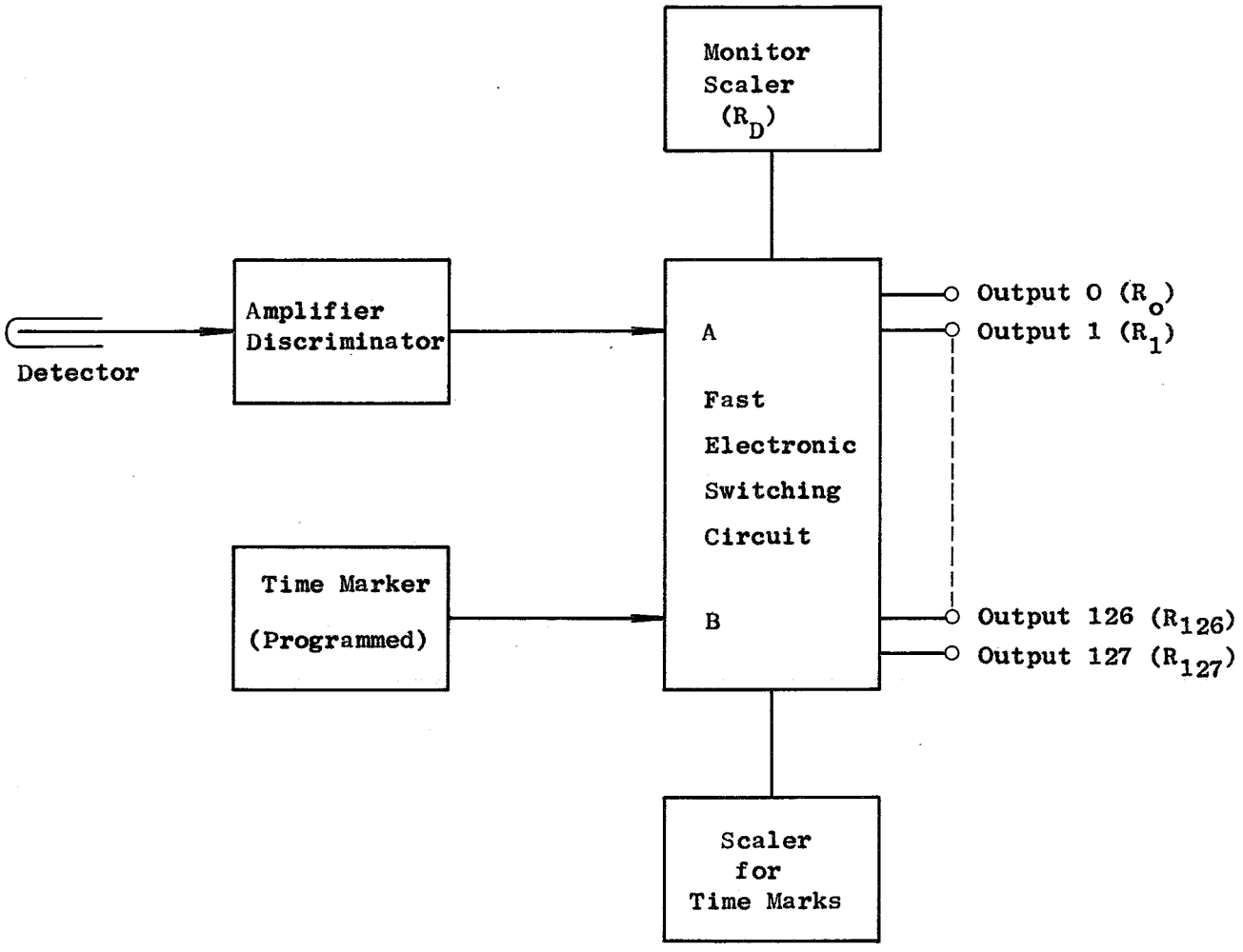

FIG.8 Schematic Diagram of Probability Distribution Analyzer

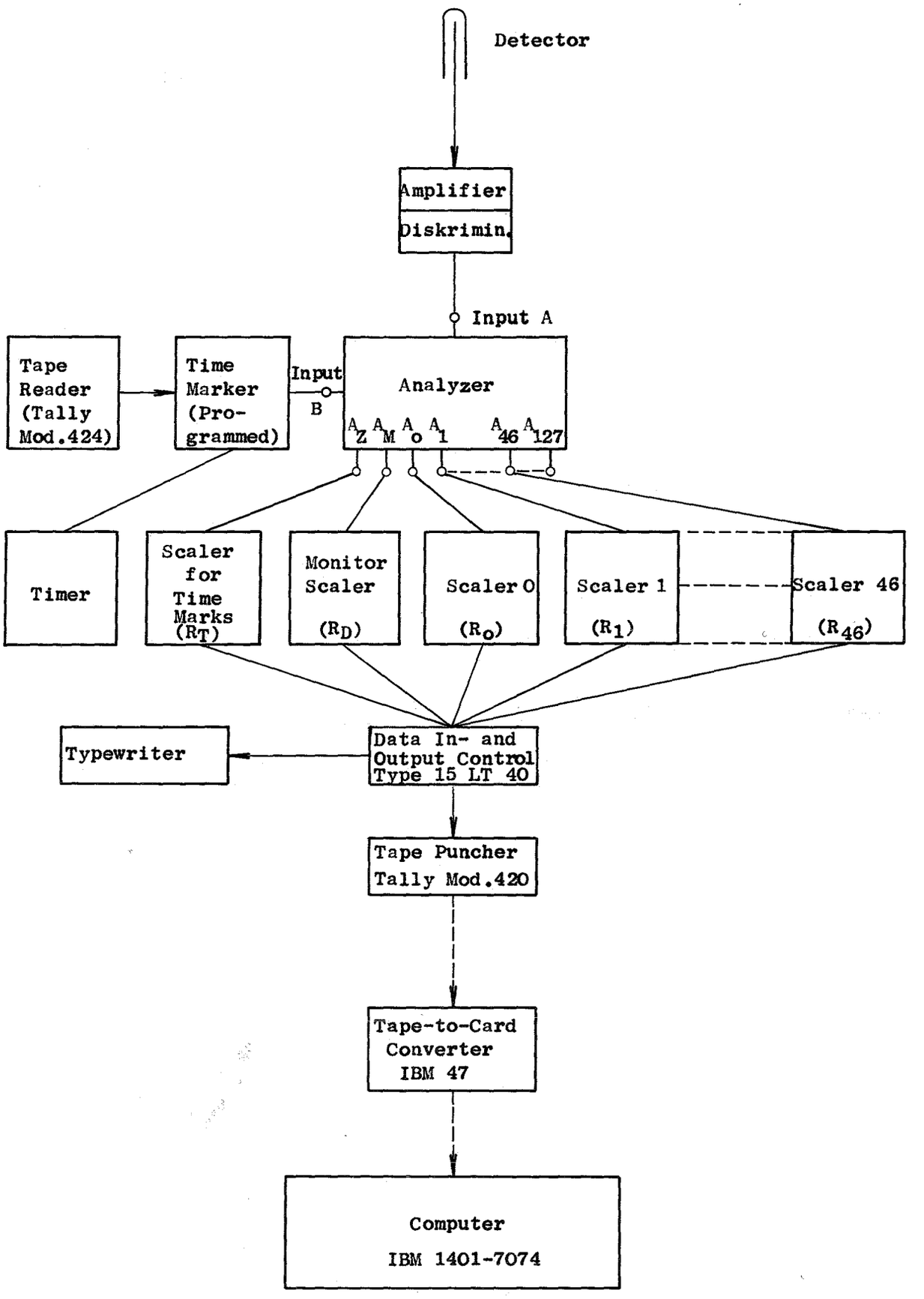

FIG.9 Blockdiagram of Data Acquisition and Reduction System

FIG.10 Measured Probability-Distributions ——————
and Equivalent POISSON-Distributions - - - - - - - - - -

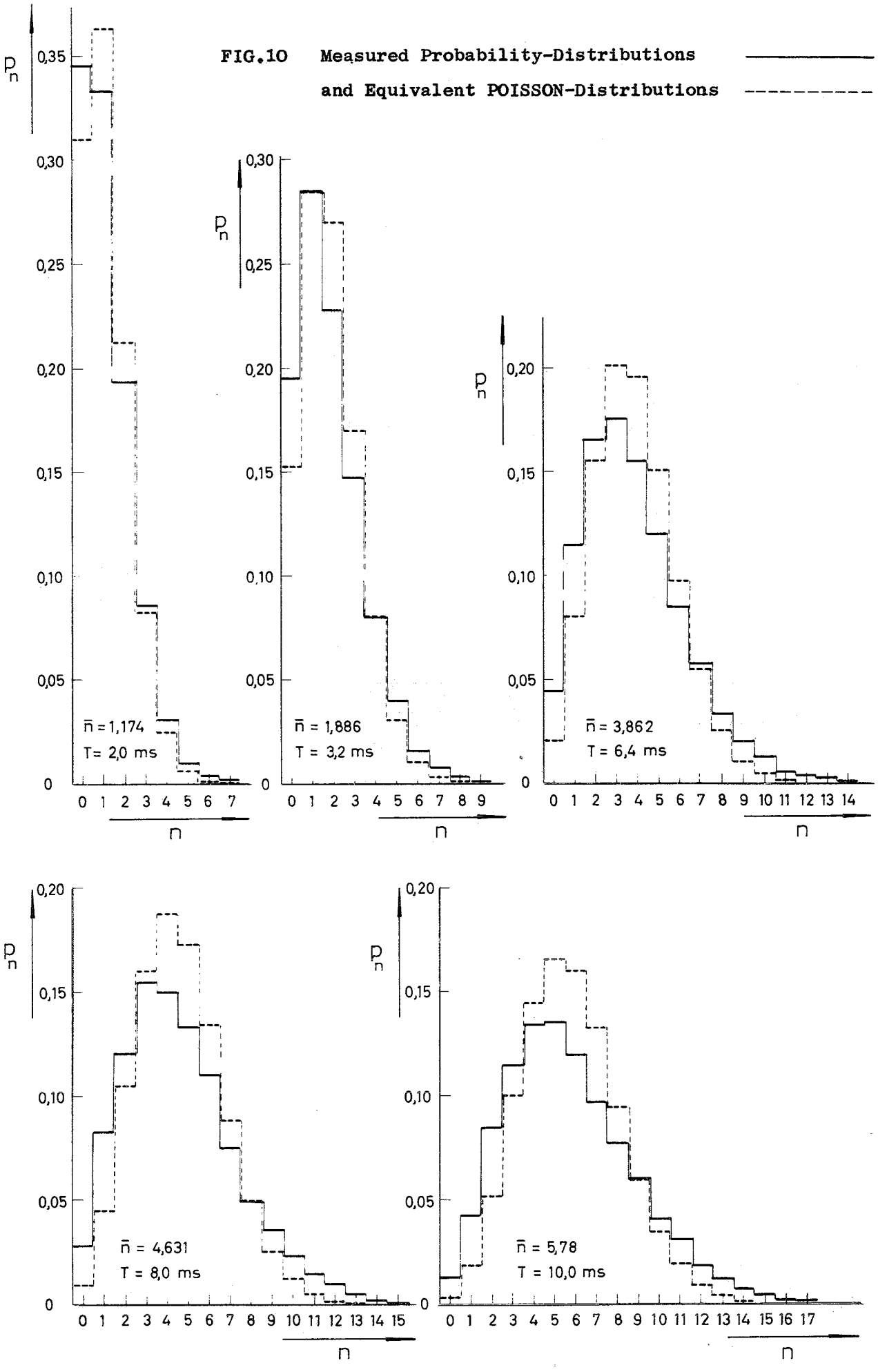

FIG.11 Deviation from the Reduced Variance of the POISSONian Distribution as Function of Interval Length